A model of bacterial toxin-dependent pathogenesis explains infective dose

Rybicki, Kisdi and Anttila 10.1073/pnas.1721061115

Supporting Information (SI)

A. Derivation and analysis of the non-spatial model. We start with the well-mixed system of the pathogen (P), toxin (T), and active immune effectors (I) governed by

$$\frac{dP}{dt} = bP(1-P) - kIP \quad [1a]$$

$$\frac{dT}{dt} = sP - mT \quad [1b]$$

$$\frac{dI}{dt} = r(I_0 - I) - eTI, \quad [1c]$$

where, as in the main text, b is the intrinsic growth rate of the pathogen, k is the rate at which an immune effector eliminates the pathogen, s and m are respectively the rates of toxin production and decay, I_0 is the constant total density of immune effectors (active and decapacitated), e is the rate at which the toxin decapacitates the active immune effectors, and r is the rate at which decapacitated immune effectors recover. In Eq. (1b), we neglect the toxin molecules that bind to an immune effector; this is an acceptable approximation when the number of toxin molecules is much higher than the number of immune effectors.

Assume that the toxin is produced and decays fast ($s, m \to \infty$) and the immune effectors are decapacitated and recover fast ($r, e \to \infty$); from Eq. (1b) and Eq. (1c), T and I then achieve the quasi-equilibrium

$$\hat{T} = \frac{sP}{m}, \quad \hat{I} = \frac{I_0}{1 + \frac{es}{rm}P}.$$

Substituting $\hat{I}$ into Eq. (1a) and using the dimensionless parameters $\xi = \frac{kI_0}{b}$ and $\chi = \frac{es}{rm}$, we get the pathogen dynamic

$$\frac{dP}{dt} = bP\left[1 - P - \frac{\xi}{1+\chi P}\right] \quad [2]$$

given in the main text.

Apart from the pathogen-free equilibrium $P_0 = 0$, Eq. (2) can have up to two positive equilibria given by

$$P_{1,2} = \frac{\chi - 1 \pm \sqrt{(\chi-1)^2 - 4\chi(\xi-1)}}{2\chi}. \quad [3]$$

We use P_1 to denote the smaller ("−") root and P_2 for the greater ("+") root.

If $\xi < 1$, then P_1 is negative and only P_2 is positive; the dynamics in Eq. (2) is attracted to P_2 irrespectively of the initial (positive) population size of the pathogen (this is easy to see directly from Eq. (2), given that the last term in the brackets is between zero and $\xi < 1$). The condition $\xi < 1$ is equivalent to $b > kI_0$, which means that the pathogen can grow even if all immune effectors are actively killing it (cf. Eq. (1a)), i.e., the pathogen does not depend on the toxin.

If $\xi > 1$ and $\chi > \chi_0(\xi) = 2\xi - 1 + 2\sqrt{\xi(\xi-1)}$, then both roots $P_{1,2}$ are positive, and the pathogen dynamics exhibits an Allee effect. At low pathogen densities, where the toxin concentration $\hat{T}$ is negligible and therefore almost all immune effectors are active, the pathogen population declines towards the asymptotically stable equilibrium P_0 (cf. in Eq. (2) for small P, the bracketed terms are approximately $1-\xi < 0$). For $P_1 < P < P_2$, however, the pathogen population grows and equilibrates at the asymptotically stable equilibrium P_2; the unstable equilibrium P_1 is the Allee threshold. This scenario occurs when the pathogen cannot grow without the toxin ($\xi > 1$) and the effect of the toxin is strong ($\chi > \chi_0(\xi)$); recall that high χ is equivalent to an efficient toxin (high e) produced in large quantities (high s) that decays only slowly (low m) and decapacitates the immune effectors for a long time (low r). If $\xi > 1$ and $\chi < \chi_0(\xi)$, then $P_{1,2}$ are negative or complex, and the pathogen-free equilibrium P_0 is the only attractor; the pathogen population dies out because its toxin is not sufficiently strong to overcome the immune effectors.

Differentiating the Allee threshold P_1 with respect to χ, it is easy to see that the derivative has the same sign as $2\chi(1-\xi-P_1)$, which is clearly negative when the system has an Allee effect, i.e., when $\xi > 1$ and $P_1 > 0$. Hence decreasing χ, for example by increasing the toxin removal rate m, increases P_1, the minimum initial density of the pathogen necessary for its spread. When χ becomes as low as $\chi_0(\xi)$, the two positive equilibria $P_{1,2}$ collide and disappear in a fold bifurcation.

B. Derivation and analysis of the reaction-diffusion model. To embed the above system into a spatial reaction-diffusion model, let $P(x,t)$, $T(x,t)$ and $I(x,t)$ denote respectively the density of pathogens, toxin and immune effectors at spatial location $x \in [-L, L]$ at time t. We consider a large interval ($L \to \infty$) with reflecting boundaries. The full reaction-diffusion system is given by

$$\frac{\partial P}{\partial t} = bP(1-P) - kIP + D_P\frac{\partial^2 P}{\partial x^2} \quad [4a]$$

$$\frac{\partial T}{\partial t} = sP - mT + D_T\frac{\partial^2 T}{\partial x^2} \quad [4b]$$

$$\frac{\partial I}{\partial t} = r(I_0 - I) - eTI + D_I\frac{\partial^2 I}{\partial x^2} \quad [4c]$$

where D_P, D_T and D_I are the diffusion coefficients of the pathogen, the toxin, and the immune effectors, respectively. We assume, as above, that the toxin and immune effector reactions are fast ($s, m, r, e \to \infty$).

Slow diffusion. Consider first the case when the toxin and the immune effectors diffuse slowly as compared to their reaction speeds (i.e., D_T and D_I are finite). In this case, the diffusion terms in Eq. (4b) and Eq. (4c) are negligible, and the toxin and immune effectors attain their local quasi-equilibria

$$\hat{T}(x,t) = \frac{sP(x,t)}{m}, \quad \hat{I}(x,t) = \frac{I_0}{1 + \frac{es}{rm}P(x,t)}.$$

Substituting $\hat{I}(x,t)$ into Eq. (4a), we arrive at

$$\frac{\partial P}{\partial t} = bf(P) + D_P \frac{\partial^2 P}{\partial x^2} \text{ with } f(P) = P\left[1 - P - \frac{\xi}{1+\chi P}\right],$$

where $\xi = \frac{kI_0}{b}$ and $\chi = \frac{es}{rm}$ as above.

We seek a travelling wave solution to this partial differential equation following Murray (1) (see Vol. 1, 13.1–13.2, 13.5). We assume that the pathogen inoculum develops such that in an interval around the center of the inoculum, i.e., near $x = 0$, the pathogen density attains the stable positive equilibrium P_2 given in Eq. (3), whereas far from the center on each side, the pathogen is absent; these two regimes are connected by a wavefront on each side of the center that may move at a constant speed outwards (the pathogen spreads by occupying more and more space) or inwards to the center (the space occupied by the pathogen shrinks and the pathogen dies out).

Let c denote the speed of the travelling wave on the right of the center; $c > 0$ corresponds to a spreading pathogen (the right wavefront moves further to the right), whereas $c < 0$ corresponds to a shrinking pathogen population (the right wavefront moves to the left, i.e., closer to the center). Let $z = x - ct$ be the spatial coordinate in the frame co-moving with the wave. Substituting $P(t,x) = P(0, x - ct) =: \tilde{P}(z)$ (where the function $\tilde{P}$ describes the constant shape of the wavefront) into the partial differential equation, we obtain

$$bf(\tilde{P}(z)) + c\tilde{P}'(z) + D_P\tilde{P}''(z) = 0,$$

where $\tilde{P}'(z)$ and $\tilde{P}''(z)$ denote the first and second derivatives of $\tilde{P}(z)$. Multiplying with $\tilde{P}'(z)$ and integrating for z between 0 and L yields

$$b\int_0^L f(\tilde{P}(z))\frac{d\tilde{P}}{dz}dz + c\int_0^L (\tilde{P}'(z))^2 dz + D_P\int_0^L \tilde{P}''(z)\tilde{P}'(z)dz = 0.$$

Since $\tilde{P}(0) = P_2$ and $\tilde{P}(L) = 0$, the first integral in this equation equals $-\int_0^{P_2} f(\tilde{P})d\tilde{P}$; and with integration by parts and using $\tilde{P}'(0) = \tilde{P}'(L) = 0$, the last integral is easily shown to be zero. The speed of the travelling wave is therefore

$$c = \frac{b\int_0^{P_2} f(\tilde{P})d\tilde{P}}{\int_0^L (\tilde{P}'(z))^2 dz}.$$

Since the denominator of this expression is clearly positive, the sign of the speed is given by the sign of the integral in the numerator. Substituting $f(P)$, we obtain that the sign of c is the same as the sign of

$$\Phi(\chi,\xi) = \frac{1}{2}P_2^2 - \frac{1}{3}P_2^3 - \frac{\xi}{\chi}P_2 + \frac{\xi}{\chi^2}\ln(1+\chi P_2)$$

(recall that P_2 is determined by ξ and χ, cf. Eq. (3)).

Fig S1 shows the sign plot of $\Phi(\chi,\xi)$, together with the behaviour of the non-spatial model. When there is an Allee effect, the pathogen may go extinct in the diffusion model even if initially it is close to its stable positive equilibrium P_2 in much of the space it occupies. The reason for this is that the Allee effect erodes the population at the leading edge of the wavefront, which is below the Allee threshold and is therefore a sink; as diffusion replenishes the population at the edge, it creates a net flux to the sink. Importantly, with slow diffusion the fate of the pathogen does not depend on its initial dose (beyond the assumption that it attains the travelling wave form).

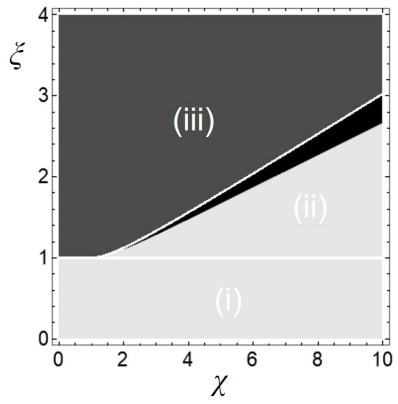

Fig. S1. The dynamics of the pathogen with slow diffusion (shading) and in the non-spatial model (areas separated by the white lines). The shading shows the sign plot of $\Phi(\chi,\xi)$; light: $\Phi(\chi,\xi) > 0$, the pathogen spreads; black: $\Phi(\chi,\xi) < 0$, the pathogen dies out; dark grey: there is no positive equilibrium P_2. The areas separated by the white lines correspond to (i) $\xi < 1$, (ii) $\xi > 1$ and $\chi > \chi_0(\xi)$, and (iii) $\xi > 1$ and $\chi < \chi_0(\xi)$. In (i), the pathogen can grow also without the toxin. In (ii), the pathogen has an Allee effect; while it has a positive equilibrium in the non-spatial model, it may spread (light part of (ii)) or die out (black part of (ii)) in the diffusion model. In (iii), the pathogen dies out in both models.

Fast diffusion. Here we assume that the diffusion of the toxin is very fast ($D_T \gg mL^2$), so that the toxin concentration quickly homogenizes over the entire space. (D_I may be arbitrary, since the fast reactions in Eq. (4c) homogenize the active immune effectors with or without their diffusion.) The total amount of toxin produced by a given pathogen population is the same as with slow diffusion, but this total is evenly distributed over the interval $[-L, L]$, so that the local quasi-equilibrium is given everywhere by

$$\hat{T}(t) = \frac{s\bar{P}(t)}{m}, \quad \hat{I}(t) = \frac{I_0}{1+\chi\bar{P}(t)},$$

where

$$\bar{P}(t) = \int_{-L}^{L} P(x,t)dx/2L$$

is the average pathogen density over the entire space at time t. Integrating Eq. (4a) over space, we obtain the dynamics of the average pathogen density as

$$\frac{d\bar{P}}{dt} = (b - k\hat{I}(t))\bar{P}(t) - \frac{b}{2L}\int_{-L}^{L}[P(t,x)]^2 dx \qquad [5]$$

(with reflecting boundaries, diffusion does not affect the total size of the population). By Jensen's inequality, we have

$$\frac{1}{2L}\int_{-L}^{L}[P(t,x)]^2 dx \geq \left[\bar{P}(t)\right]^2$$

so that the solution of Eq. (5) is bounded from above by the solution of

$$\frac{d\bar{P}}{dt} = \left[b - k\hat{I}(t) - b\bar{P}(t)\right]\bar{P}(t)$$
$$= b\bar{P}(t)\left[1 - \bar{P}(t) - \frac{\xi}{1+\chi\bar{P}(t)}\right],$$

which is the same as the non-spatial dynamics in Eq. (2). Hence if the pathogen needs to decapacitate the immune system for its growth ($\xi > 1$), then it cannot spread unless $\chi > \chi_0(\xi)$ and the pathogen's initial average density $\bar{P}(0)$ exceeds the Allee threshold P_1. Note that this condition is not sufficient; if the initial distribution of the pathogen is not homogeneous (which is likely), then Jensen's inequality is a strict inequality, and the pathogen population can go extinct even if $\bar{P}(0) > P_1$.

With slow diffusion, the pathogen population density has to be above the Allee threshold only locally, which can be achieved with a small initial dose; if a travelling wave solution is achieved, the spread of the pathogen does not depend on the size of its population. In contrast, with fast diffusion, the global spatial average density of the pathogen matters, so that the initial number of pathogens must exceed $2LP_1$; this is a high dose that scales with the size of the host, L.

C. Details of the stochastic spatial model.

Tophat kernels. A kernel $K(\mathbf{x},\mathbf{y}) = h \cdot f(\mathbf{x},\mathbf{y})$ is defined in the terms of its total rate h and a density function $f(\mathbf{x},\mathbf{y})$ describing how the rates are distributed across space. In our simulations, we used tophat kernels, which are defined as

$$K_{\ell,h}(\mathbf{x},\mathbf{y}) = \begin{cases} h/(\pi\ell^2) & \text{if } \operatorname{dist}(\mathbf{x},\mathbf{y}) \le \ell \\ 0 & \text{otherwise,} \end{cases}$$

where $\operatorname{dist}(\mathbf{x},\mathbf{y})$ is the Euclidean distance between the two points $\mathbf{x}$ and $\mathbf{y}$ in the simulation space with periodic boundary conditions, ℓ is the length scale, and the total rate is h.

The existing particles are delta-peaks at known locations. When we integrate these with the kernel $h \cdot f(\mathbf{x},\mathbf{y})$, we arrive at the rates given in the Materials and Methods section of the main text. For example, a pathogen at location $\mathbf{x}$ consumes a tissue particle at location $\mathbf{y}$ at the rate

$$C(\mathbf{x},\mathbf{y}) = b\int_{\mathcal{H}}\int_{\mathcal{H}} f(\mathbf{x},\mathbf{y})\delta_{\mathbf{x}}\delta_{\mathbf{y}}d\mathbf{x}d\mathbf{y},$$

which is $b/(\pi\ell_C^2)$ if $\operatorname{dist}(\mathbf{x},\mathbf{y}) \le \ell_C$ and zero otherwise. For movement and for the birth of a new particle (pathogen reproduction or toxin production), however, retaining the density function $f(\mathbf{x},\mathbf{y})$ is essential; since space is continuous, the probability that a jump (or birth) takes a particle from its known position $\mathbf{x}$ to a specific point $\mathbf{y}$ is zero, but the probability of landing in a small neighbourhood U of point $\mathbf{y}$ is positive and is given by $f(\mathbf{x},\mathbf{y}) \cdot |U|$, where $|U|$ is the area of the neighbourhood.

Spatial reactions. To describe the reactions in the spatial setting, we extend the usual reaction rate equations to consider also the locations of particles. We use the notation

$$\underset{\mathbf{x}}{\mathrm{A}} \xrightarrow{K(\mathbf{x},\mathbf{y})} \underset{\mathbf{y}}{\mathrm{A}}$$

to mean that particle A moves from its known location $\mathbf{x}$ to a neighbourhood of $\mathbf{y}$ according to the kernel $K(\mathbf{x},\mathbf{y})$. Thus, the reaction rate equation can be interpreted as follows: particle A at location $\mathbf{x}$ jumps at rate h, and when the jump event occurs, a new location $\mathbf{y}$ is sampled from distribution given by the probability density function $f(\mathbf{x},\mathbf{y})$. In the case of tophat kernels, the new location is sampled uniformly at random from a disk of radius ℓ centered at the starting point $\mathbf{x}$, where ℓ is the length scale of K. For a process involving the interaction of two particles, we write

$$\underset{\mathbf{x}}{\mathrm{A}} + \underset{\mathbf{y}}{\mathrm{B}} \xrightarrow{R(\mathbf{x},\mathbf{y})\cdot f(\mathbf{x},\mathbf{z})} \underset{\mathbf{z}}{\mathrm{C}}$$

to denote that particle of type A at $\mathbf{x}$ and particle of type B at $\mathbf{y}$ react at rate $R(\mathbf{x},\mathbf{y})$ to produce a new particle of type C that appears at a random location $\mathbf{z}$, where $f(\mathbf{x},\mathbf{z})$ is the probability density of the location of the new individual. Using this notation, we can write down the spatial versions of the basic reactions, which are given in Table S1.

Initialisation of the model. The baseline parameter values used for the simulations reported in the main text are in Table S2. Fig S2 illustrates how a simulation replicate is initialised. At time $t = 0$, the focal area contains tissue particles (H) and immune effectors in the seek state (IS). These particles follow complete spatial randomness with densities $\rho_{\mathrm{H}} = 3/2$ and $\rho_{\mathrm{IS}} = 1/2$ per unit area, respectively. The initial inoculum of the pathogen is introduced onto an *inoculation area* which is a circle of radius κ. The locations of the pathogen individuals are sampled uniformly at random within the inoculation area. The parameter κ controls the size of the inoculation area, that is, it determines the level of initial spatial aggregation of the pathogens.

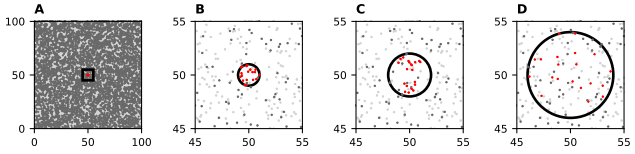

Fig. S2. Examples of the initial state of the system. Dark gray points represent immune effectors (IS) and light gray points tissue particles (H). Red points are pathogen particles. **A.** The entire simulation space (i.e.the focal area) is a torus of size 100×100. The black rectangle represents a 10×10 part shown in the next three panels. **B.** The initial dose of 20 pathogens is introduced into an inoculation area with radius $\kappa = 1$ represented by the black circle. **C.** The same initial dose of 20 pathogen particles introduced into an inoculation area with radius $\kappa = 2$. **D.** The initial dose is introduced into an inoculation area with radius $\kappa = 4$.

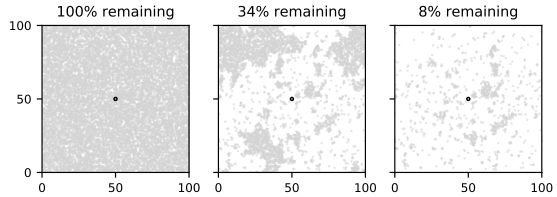

Fig. S3. Examples of scenarios where no tissue has been consumed (left), 66% of tissue has been consumed (center), and over 90% of the tissue has been consumed (right). The small circle denotes the initial inoculation area of radius $\kappa = 1$. The snapshots are from a simulation with toxin diffusion scale $\ell_{\mathrm{T}} = 1$ and the initial dose of one pathogen individual.

Table S1. Complete list of reactions in the stochastic individual-based spatial model.

$\underset{\mathbf{x}}{\mathrm{P}} + \underset{\mathbf{y}}{\mathrm{H}} \xrightarrow{C(\mathbf{x},\mathbf{y})\cdot f(\mathbf{x},\mathbf{z})} \underset{\mathbf{x}}{\mathrm{P}} + \underset{\mathbf{z}}{\mathrm{P}}$	pathogen at $\mathbf{x}$ consumes tissue from $\mathbf{y}$ and produces an offspring to $\mathbf{z}$,
$\underset{\mathbf{x}}{\mathrm{P}} + \underset{\mathbf{y}}{\mathrm{IK}} \xrightarrow{K(\mathbf{x},\mathbf{y})} \underset{\mathbf{x}}{\mathrm{IK}}$	immune effectors in the 'kill' state eliminate pathogens,
$\underset{\mathbf{x}}{\mathrm{P}} \xrightarrow{S(\mathbf{x},\mathbf{y})} \underset{\mathbf{x}}{\mathrm{P}} + \underset{\mathbf{y}}{\mathrm{T}}$	pathogens secrete toxins into their surroundings,
$\underset{\mathbf{x}}{\mathrm{IS}} + \underset{\mathbf{y}}{\mathrm{T}} \xrightarrow{E(\mathbf{x},\mathbf{y})} \underset{\mathbf{x}}{\mathrm{ID}}$	toxins decapacitate immune effectors and are consumed in the process,
$\underset{\mathbf{x}}{\mathrm{T}} \xrightarrow{m} \emptyset$	toxins become inactive and are removed,
$\underset{\mathbf{x}}{\mathrm{IS}} + \underset{\mathbf{y}}{\mathrm{P}} \xrightarrow{A(\mathbf{x},\mathbf{y})} \underset{\mathbf{x}}{\mathrm{IK}} + \underset{\mathbf{y}}{\mathrm{P}}$	IEs detect pathogens and go to "kill" state,
$\underset{\mathbf{x}}{\mathrm{IK}} \xrightarrow{q} \underset{\mathbf{x}}{\mathrm{IS}}$	IEs in "kill" state switch to "seek" state,
$\underset{\mathbf{x}}{\mathrm{ID}} \xrightarrow{r} \underset{\mathbf{x}}{\mathrm{IS}}$	decapacitated immune effectors recover from the effects of the toxin,
$\underset{\mathbf{x}}{\mathrm{P}} \xrightarrow{D_{\mathrm{P}}(\mathbf{x},\mathbf{y})} \underset{\mathbf{y}}{\mathrm{P}}$	pathogens move according to the kernel D_{P},
$\underset{\mathbf{x}}{\mathrm{T}} \xrightarrow{D_{\mathrm{T}}(\mathbf{x},\mathbf{y})} \underset{\mathbf{y}}{\mathrm{T}}$	toxins move according to the kernel D_{T},
$\underset{\mathbf{x}}{\mathrm{IS}} \xrightarrow{D_{\mathrm{IS}}(\mathbf{x},\mathbf{y})} \underset{\mathbf{y}}{\mathrm{IS}}$	immune effectors in the seek state move according to the kernel D_{IS},
$\underset{\mathbf{x}}{\mathrm{IK}} \xrightarrow{D_{\mathrm{IK}}(\mathbf{x},\mathbf{y})} \underset{\mathbf{y}}{\mathrm{IK}}$	immune effectors in the kill state move according to the kernel D_{IK}.

Above $f(\mathbf{x},\mathbf{z})$ is the probability density function in $D_{\mathrm{P}} = h \cdot f(\mathbf{x},\mathbf{z})$.

Recording the simulation outcomes. In all experiments, we simulated the model until (a) all pathogens were killed or (b) all tissue particles were consumed. We recorded the configuration of the system, i.e., the locations $\Omega_X(t)$ of each particle of type X (P, T, H, IS, IK or ID) every $\Delta t = 1$ time units. We calculated the fraction of tissue particles remaining in the focal area at the end of the simulation. Fig S3 shows examples where different amounts of the host tissue has been consumed.

Table S2. Parameters of the spatial model.

Process	Kernel	Rate (h)	Length scale (ℓ)
Toxin secretion	S	$s = 1$	ℓ_{T}
Toxin effectivity	E	$e = 1$	1
Tissue consumption	C	$b = 1$	1
IE (kill) elimination	K	$k = 1.75$	3
IE (seek) activation	A	$a = 1$	1
Toxin movement	D_{T}	1	ℓ_{T}
Parasite movement	D_{P}	1	1
IE (seek) movement	D_{IS}	1	10
IE (kill) movement	D_{IK}	1	1
Toxin removal	–	$m = 1$	–
Immune effector recovery rate	–	$r = 0.025$	–
Transition from 'kill' state to 'seek'	–	$q = 0.2$	–

D. Sensitivity analysis of the model.

Setup of the sensitivity analysis. We conducted a sensitivity analysis of the stochastic spatial model by varying the model parameters, excluding the movement rates, by ±10%, ±25% and ±50% deviations (see Table S3). For the sensitivity analysis, we used the smallest inoculation area with $\kappa = 1$, and repeated the analysis for two values for the toxin movement scale parameter, $\ell_{\mathrm{T}} = 1$ (local action) and $\ell_{\mathrm{T}} = 32$ (distant action). We simulated 1000 replicates for the initial doses of 10^d particles for $d \in \{0, 1, 2, 3, 4, 4.5\}$. For the toxin removal rate m, we also examined the case $m = 0.01$.

Results of the sensitivity analysis. Fig S4, Fig S5, and Fig S6 show the results of the sensitivity analysis. We make the following observations:

- In all cases, the qualitative pattern remains the same when the deviations are ±10% and ±25%; locally acting toxins lead to stronger response at low initial doses than distantly acting toxins. For large deviations of ±50% the pattern is sometimes less apparent.
- The model is sensitive to the initial densities of tissue and immune effectors, but the results are as expected: the pathogens do better when they have more nutrients available and they are worse off if the number of immune effector grows.
- We see that the model is sensitive to the length scales of some kernels. For example, increasing the length scale of the pathogen movement kernel benefits the pathogens. This is natural, as they can then escape the immune effectors more easily and move into areas with unconsumed nutrients. The latter also explains why increasing length scale of tissue consumption has a strong effect as well.

E. Effects of aggregation on the distribution of outcomes.

Figure 2 of the main text shows the distribution of outcomes for an inoculation area with radius $\kappa = 1$. Fig S7, Fig S8, and Fig S9 show the distribution of outcomes with radii $\kappa = 4, 8, 16$, respectively.

Table S3. Parameter values for the sensitivity analysis

Parameter name	Baseline	+10%	−10%	+25%	−25%	+50%	−50%
Tissue consumption rate b	1.0	1.1	0.9	1.25	0.75	1.5	0.5
Toxin effectivity rate e	1.0	1.1	0.9	1.25	0.75	1.5	0.5
Toxin removal rate m	1.0	1.1	0.9	1.25	0.75	1.5	0.5
Toxin secretion rate s	1.0	1.1	0.9	1.25	0.75	1.5	0.5
Initial tissue density ρ_{P}	1.5	1.65	1.35	1.875	1.125	2.25	0.75
Initial seeker density ρ_{IS}	0.5	0.55	0.45	0.625	0.375	0.75	0.25
IE (kill) elimination rate k	1.75	1.925	1.575	2.1875	1.3125	2.625	0.875
Immune effector recovery rate r	0.025	0.0275	0.0225	0.03125	0.01875	0.0375	0.0125
Kill to seek rate q	0.2	0.22	0.18	0.25	0.15	0.3	0.1
Tissue consumption scale	1.0	1.1	0.9	1.25	0.75	1.5	0.5
Toxin effectivity scale	1.0	1.1	0.9	1.25	0.75	1.5	0.5
IE (kill) elimination scale	3	3.3	2.7	3.75	2.25	4.5	1.5
Parasite movement scale	1	1.1	0.9	1.25	0.75	1.5	0.5
IE (seek) movement scale	10	11	9	12.5	7.5	15	5
IE (kill) movement scale	1	1.1	0.9	1.25	0.75	1.5	0.5
IE activation scale	1	1.1	0.9	1.25	0.75	1.5	0.5

F. Analysis of the data. The data analysis and figures were done using R version 3.3.2 (2) with ggplot2 (3), and matplotlib 2.0 (4). The average dose-response line in Fig 2, Fig S7, Fig S8, and Fig S9 was fitted to the modified Hill equation

$$f(x) = a + b \cdot \frac{(x/c)^p}{1 + (x/c)^p},$$

where a is the minimum response, b the maximum response, c the half-saturation constant, and p is the steepness of the response. Note that the usual Hill equation has $a = 0$ and $b = 1$. However, in our simulations, the doses consist of discrete particles, and hence, the minimum dose of 1 particle already has a positive probability of consuming tissue particles (yielding a positive response).

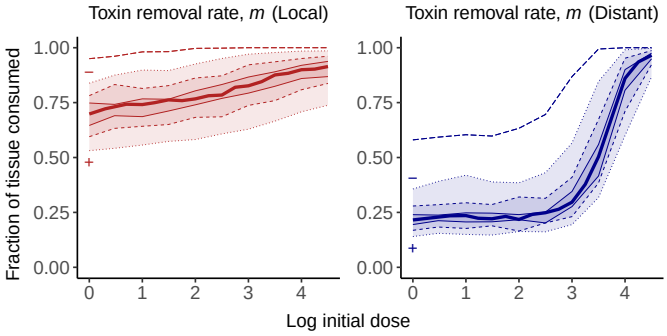

Fig. S4. Model sensitivity analysis for the toxin removal rate m for both local ($\ell_{\mathrm{T}} = 1$, left) and distant ($\ell_{\mathrm{T}} = 32$, right) action. The horizontal axis is the dose, and the vertical axis is the average fraction of tissue consumed (averaged over all replicates). The thick lines denote the baseline parameterisation, the thin solid line 10% deviation, the dashed line 25% deviation, and the dotted line 50% deviation. The + symbol is above the baseline (and – below) if increasing the parameter value increases the response variable (average fraction of tissue consumed). The colour fill simply indicates the area that remains between the thin lines (i.e. the larger the filled area, the more sensitive the model is to a particular parameter). The top dashed line is the experiment with $m = 0.01$.

S1 Video. Animation: low dose, local mechanism. Animation illustrating how the dynamics of the model evolve over time with a low initial dose of a locally acting pathogen. The parameters and colours are as in first row of Fig 1 in the main text.

S2 Video. Animation: low dose, distant mechanism. Animation illustrating how the dynamics of the model evolve over time with a low initial dose of a distantly acting pathogen. The parameters and colours are as in second row of Fig 1.

S3 Video. Animation: high dose, local mechanism. Animation illustrating how the dynamics of the model evolve over time with a high initial dose of a locally acting pathogen. The parameters and colours are as in third row of Fig 1.

S4 Video. Animation: high dose, distant mechanism. Animation illustrating how the dynamics of the model evolve over time with a high initial dose of a distantly acting pathogen. The parameters and colours are as in fourth row of Fig 1.

1. Murray JD (2002) *Mathematical Biology.* (Springer-Verlag New York).
2. R Core Team (2016) *R: A Language and Environment for Statistical Computing* (R Foundation for Statistical Computing, Vienna, Austria).
3. Wickham H (2009) *ggplot2: Elegant Graphics for Data Analysis.* (Springer-Verlag New York).
4. Hunter JD (2007) Matplotlib: A 2d graphics environment. *Comput Sci Eng* 9(3):90–95.

SI Video Captions.

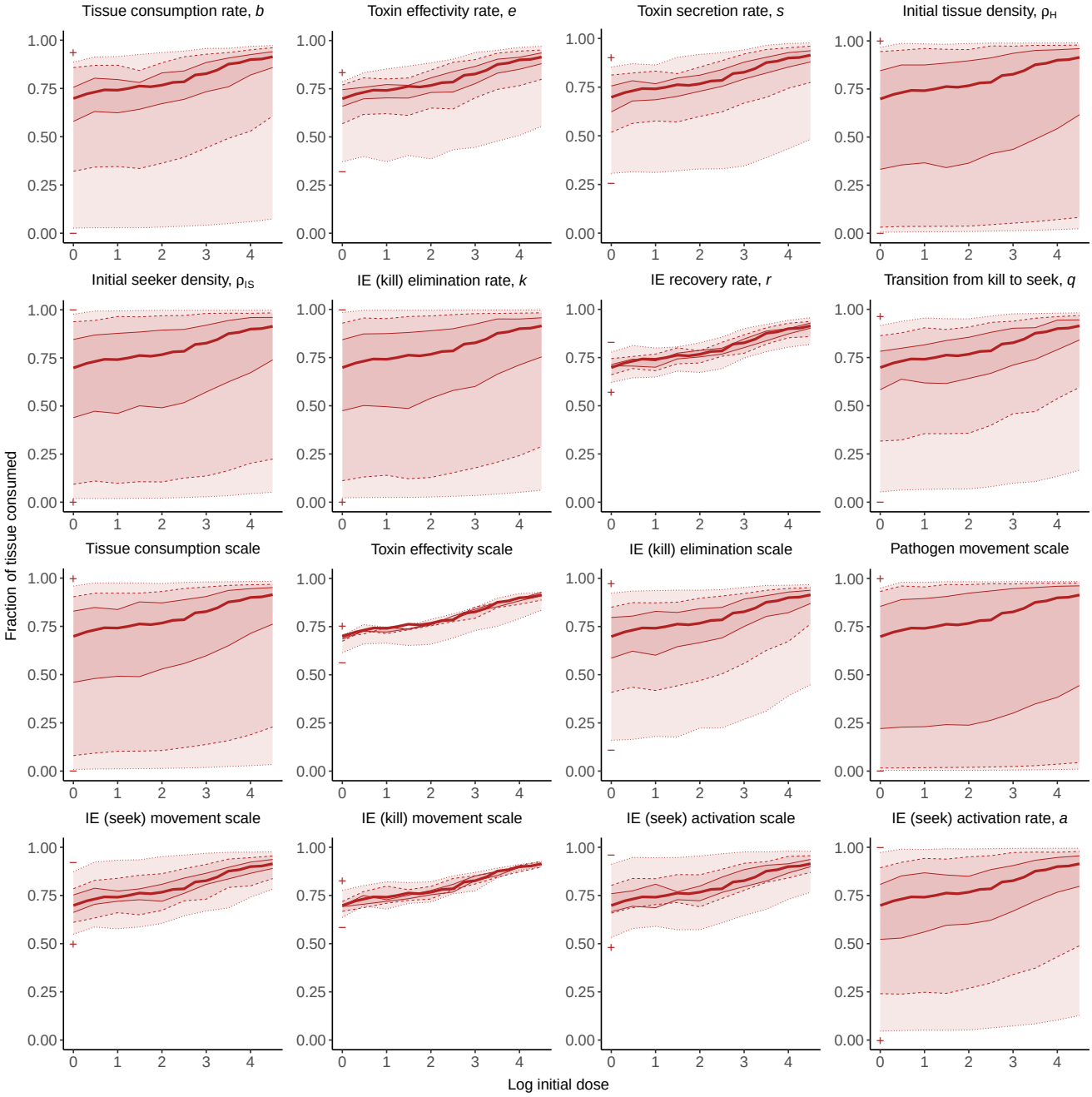

Fig. S5. Results of the sensitivity analysis for local action ($\ell_{\mathrm{T}} = 1$). The horizontal axis is the dose, and the vertical axis is the average fraction of tissue consumed (averaged over all replicates). The thick lines denote the baseline parameterisation, the thin solid line 10% deviation, the dashed line 25% deviation, and the dotted line 50% deviation. The + symbol is above the baseline (and – below) if increasing the parameter value increases the response variable (average fraction of tissue consumed). The colour fill simply indicates the area that remains between the thin lines (i.e. the larger the filled area, the more sensitive the model is to a particular parameter).

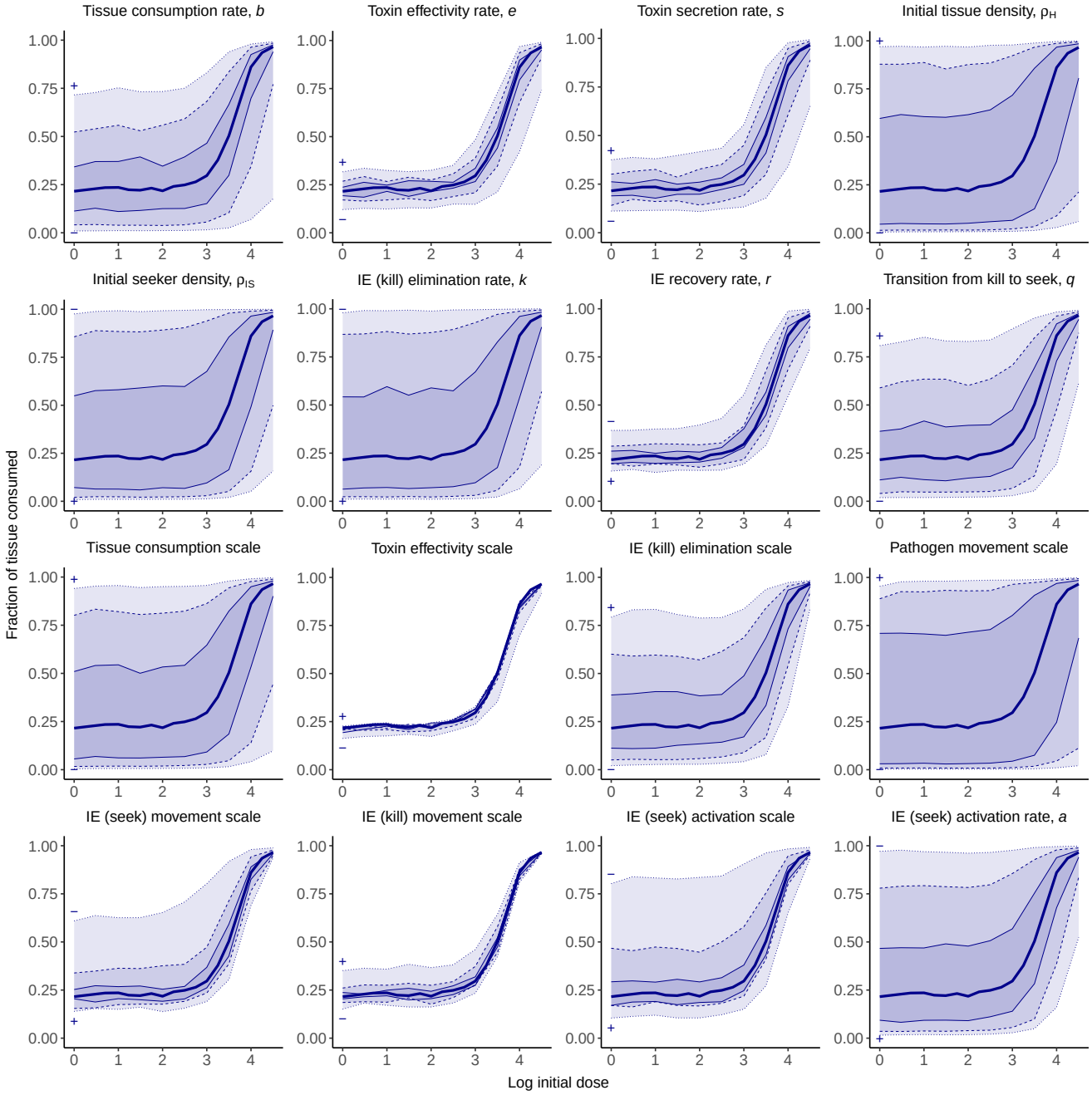

Fig. S6. Results of the sensitivity analysis for distant action ($\ell_{\mathrm{T}} = 32$). The horizontal axis is the dose, and the vertical axis is the average fraction of tissue consumed (averaged over all replicates). The thick lines denote the baseline parameterisation, the thin solid line 10% deviation, the dashed line 25% deviation, and the dotted line 50% deviation. The + symbol is above the baseline (and – below) if increasing the parameter value increases the response variable (average fraction of tissue consumed). The colour fill simply indicates the area that remains between the thin lines (i.e. the larger the filled area, the more sensitive the model is to a particular parameter).

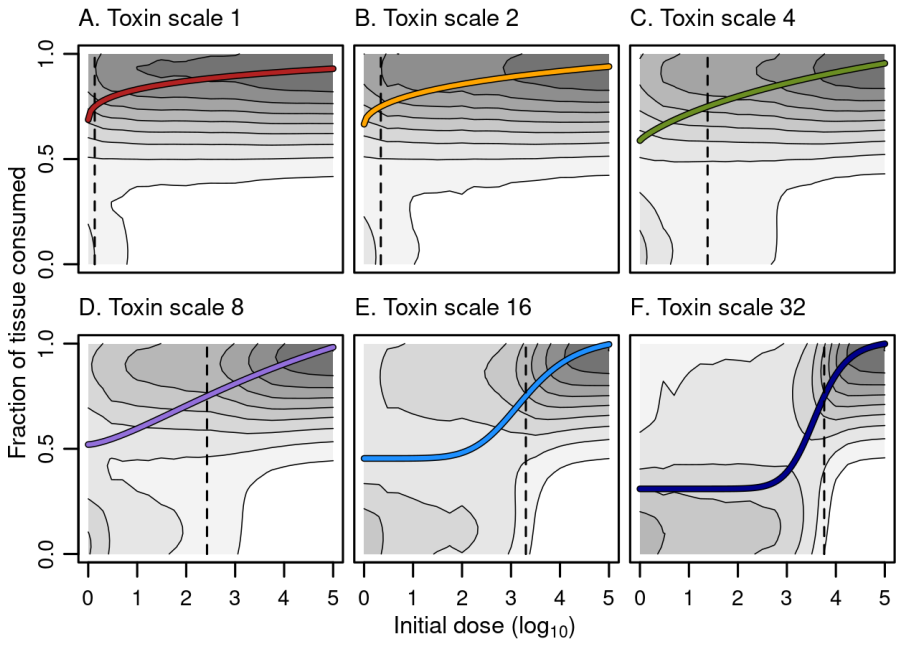

Fig. S7. The dose-response curves for different modes of action when the inoculation area has radius $\kappa = 4$. The line gives the average dose-response curve fitted to the Hill equation similarly as in Fig 2 of the main text, but is based on the same data as Fig 3B of the main text.

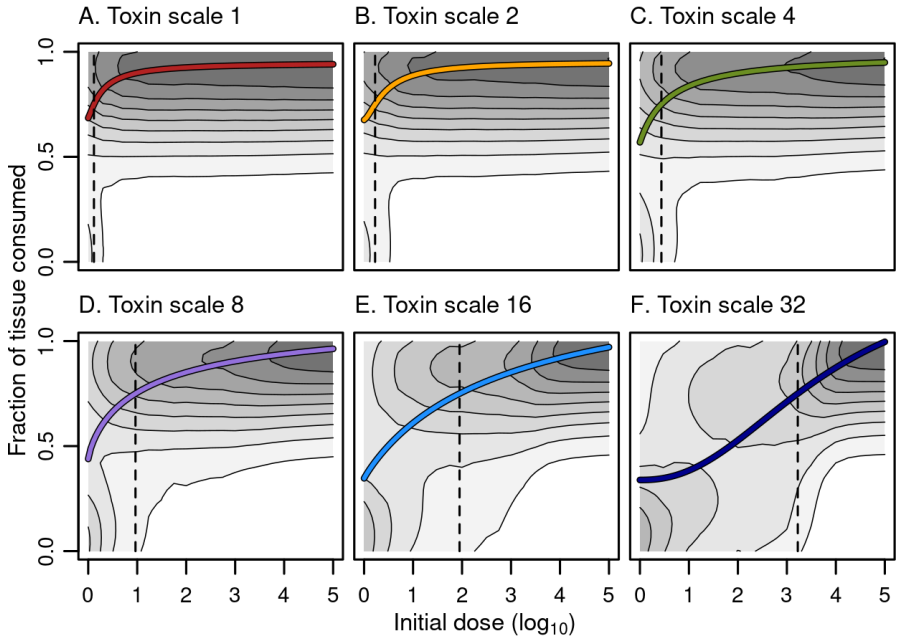

Fig. S8. The dose-response curves for different modes of action when the inoculation area has radius $\kappa = 8$. The line gives the average dose-response curve fitted to the Hill equation similarly as in Fig 2 of the main text, but is based on the same data as Fig 3C of the main text.

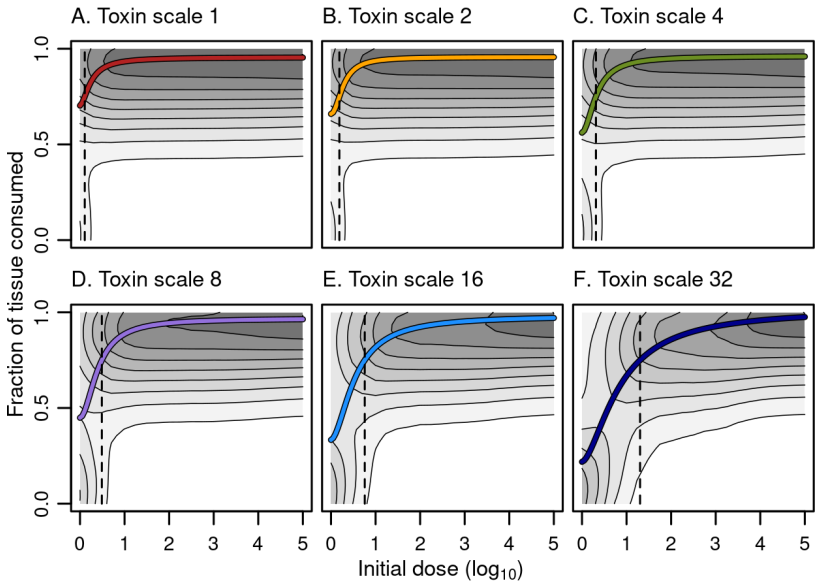

Fig. S9. The dose-response curves for different modes of action when the inoculation area has radius $\kappa = 16$. The line gives the average dose-response curve fitted to the Hill equation similarly as in Fig 2 of the main text, but is based on the same data as Fig 3D of the main text.